



Proteomic Analysis on Anti-Proliferative and Apoptosis Effects of Curcumin Analog, 1,5-bis(4-Hydroxy-3-Methoxyphenyl)-1,4-Pentadiene-3-One-Treated Human Glioblastoma and Neuroblastoma Cells

OPEN ACCESS

Yee Qian Lee¹, Pathmanathan Rajadurai¹, Faridah Abas^{2,3}, Iekhsan Othman¹ and Rakesh Naidu^{1*}

Edited by:

Mahendra Pratap Kashyap,
University of Alabama at Birmingham,
United States

Reviewed by:

Jacopo Junio Valerio Branca,
University of Florence, Italy
Chiara Giacomelli,
University of Pisa, Italy

*Correspondence:

Rakesh Naidu
kdrakeshna@hotmail.com

Specialty section:

This article was submitted to
Molecular Diagnostics
and Therapeutics,
a section of the journal
Frontiers in Molecular Biosciences

Received: 24 December 2020

Accepted: 04 March 2021

Published: 30 April 2021

Citation:

Lee YQ, Rajadurai P, Abas F,
Othman I and Naidu R (2021)
Proteomic Analysis on
Anti-Proliferative and Apoptosis
Effects of Curcumin Analog, 1,5-bis(4-
Hydroxy-3-Methoxyphenyl)-1,4-
Pentadiene-3-One-Treated Human
Glioblastoma and Neuroblastoma
Cells. *Front. Mol. Biosci.* 8:645856.
doi: 10.3389/fmolb.2021.645856

¹ Jeffrey Cheah School of Medicine and Health Sciences, Monash University Malaysia, Subang Jaya, Malaysia, ² Laboratory of Natural Products, Faculty of Science, University Putra Malaysia, Seri Kembangan, Malaysia, ³ Department of Food Science, Faculty of Food Science and Technology, University Putra Malaysia, Seri Kembangan, Malaysia

Curcumin analogs with excellent biological properties have been synthesized to address and overcome the poor pharmacokinetic profiles of curcumin. This study aims to investigate the cytotoxicity, anti-proliferative, and apoptosis-inducing ability of curcumin analog, MS13 on human glioblastoma U-87 MG, and neuroblastoma SH-SY5Y cells, and to examine the global proteome changes in these cells following treatment. Our current findings showed that MS13 induced potent cytotoxicity and anti-proliferative effects on both cells. Increased caspase-3 activity and decreased bcl-2 concentration upon treatment indicate that MS13 induces apoptosis in these cells in a dose- and time-dependent manner. The label-free shotgun proteomic analysis has defined the protein profiles in both glioblastoma and neuroblastoma cells, whereby a total of nine common DEPs, inclusive of glyceraldehyde 3-phosphate dehydrogenase (GAPDH), alpha-enolase (ENO1), heat shock protein HSP 90-alpha (HSP90AA1), Heat shock protein HSP 90-beta (HSP90AB1), Eukaryotic translation initiation factor 5A-1 (EIF5A), heterogenous nuclear ribonucleoprotein K (HNRNPK), tubulin beta chain (TUBB), histone H2AX (H2AFX), and Protein SET were identified. Pathway analysis further elucidated that MS13 may induce its anti-tumor effects in both cells via the common enriched pathways, "Glycolysis" and "Post-translational protein modification." Conclusively, MS13 demonstrates an anti-cancer effect that may indicate its potential use in the management of brain malignancies.

Keywords: glioblastoma, neuroblastoma, diarylpentanoids, cytotoxicity, anti-proliferation, apoptosis, shotgun proteomics

INTRODUCTION

Glioblastoma and neuroblastoma are the two most common neural and brain tumors among adults and children, respectively (de Weille, 2014). Glioblastoma, which is classified as Grade IV malignant gliomas by the World Health Organization (WHO) (Louis et al., 2007; Gupta and Dwivedi, 2017), has been well documented for its deadly mortality rate, with a 5-year survival rate of less than 50% (Delgado-López and Corrales-García, 2016). On the other hand, a neuroblastoma that originates from neural crest cells is well known for its heterogenous clinical outcomes, ranging from spontaneous regression to rapid metastasis with poor prognosis (Tomolonis et al., 2018). Multimodality treatment inclusive of surgery in combination with chemotherapy and radiotherapy remains as the most established therapeutic regime for both glioblastoma and neuroblastoma. Nonetheless, this therapeutic regime has yet to substantially improve the morbidity and mortality and, therefore, highlights the need for more powerful anti-cancer drugs.

Curcumin or diferuloylmethane is a hydrophobic polyphenol extracted from the rhizome of *Curcuma longa*. It is regarded as a “Generally Recognized as Safe” phytochemical by the Food and Drug Administration (FDA) with good tolerability and safety profiles. Therefore, it is widely consumed as a spice, preservative, and coloring agent in Asian countries. Additionally, it also serves as an Ayurvedic medicine for ailments such as biliary and hepatic disorders, cough, abdominal pain, and rheumatism (Chattopadhyay et al., 2004). Curcumin facilitates a wide spectrum of biological activities, including anti-inflammatory, anti-oxidant, anti-parasitic, chemo-preventive, pro-apoptotic, and anti-bacterial properties through the modulation of a plethora of signaling molecules (Chattopadhyay et al., 2004). In 1987, the cytotoxic activity of curcumin was first demonstrated on leukemic lymphocytes by Kuttan et al. (1985). Since then, increasing interest was drawn to delineate the anti-cancer effects of curcumin on other types of cancers (Choudhuri et al., 2002; Jaiswal et al., 2002; Lin et al., 2007). Noteworthy, the cytotoxic and anti-proliferative effects of curcumin on glioblastoma cells (Karmakar et al., 2007) or its xenograft models (Perry et al., 2010) are important findings, suggesting possible therapeutic intervention approaches. Studies revealed that curcumin induced its cytotoxic potential by arresting the glioblastoma cells in the G2/M phase and, in turn, increased the sensitivity of cells toward radiation (Zanotto-Filho et al., 2012; Yu et al., 2015). Additionally, apoptotic (Huang et al., 2010) and cell signaling molecules (Yu et al., 2015) were also identified as the molecular targets for curcumin in glioblastoma cells. These encouraging evidences indeed showcased the therapeutic potential of curcumin in treating glioblastoma. However, limitations such as low bioavailability, rapid degradation, and short half-life have impeded the development of curcumin as a clinical drug. In this regard, numerous strategies, including the chemical structure modification, have been envisaged by researchers to overcome the poor pharmacokinetic profiles of curcumin.

Diarylpentanoids are products of chemical modification around the α,β -unsaturated diketone group in curcumin. These curcumin analogs that bear a five-carbon spacer in between the

terminal aryl rings demonstrate better pharmacokinetic profiles and bioactivities. Several studies suggested that diarylpentanoid may be a better therapeutic option over its parent compound in treating cancers. For instance, GO-Y016, GO-Y030, and GO-Y031 demonstrated 30 times more potent growth-suppressive activity compared with curcumin, 5-fluorouracil, cisplatin, and irinotecan when treated on colorectal cancer cells (Oho et al., 2006). Another selected diarylpentanoid (MS13) used in our present study that bears a five-carbon spacer with α,β -unsaturated ketone group between the terminal aryl rings also showed consistent findings, in which up to five times lower EC_{50} was revealed when treated on prostate (Citalingam et al., 2015) and cervical (Paulraj et al., 2015) cancer cells. Moreover, this compound was also found to induce cancer cell death by activating the apoptosis pathway in gastric (Yoshida et al., 2018) and colorectal (Cen et al., 2009) cancer cells. To date, no studies have reported on the anti-cancer activities and the mode of action of MS13 in human glioblastoma and neuroblastoma cells.

Hence, this study aims to investigate the cytotoxicity, anti-proliferative, and apoptosis effects of MS13 against human glioblastoma and neuroblastoma cells. We extended our study in analyzing the differentially expressed proteins (DEPs) in human glioblastoma and neuroblastoma cells upon exposure to MS13 relative to untreated cells. The high-throughput label-free shotgun proteomic analysis revealed several commonly DEPs in both glioblastoma and neuroblastoma cells, in which these data further provided an insight into the plausible pathways modulated by MS13 as a potential anti-cancer agent in treating brain malignancies in the future. This study, we believe, is the first to investigate the anti-cancer effects of MS13 on human glioblastoma and neuroblastoma cells from the proteomic perspective.

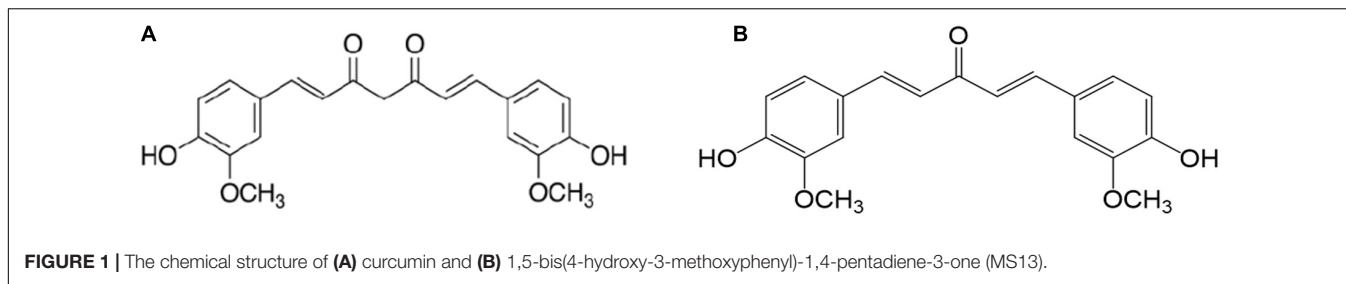
MATERIALS AND METHODS

Cell Culture and Maintenance

Human glioblastoma (U-87 MG) cell line was purchased from ElabScience® (Wuhan, China), whereas human neuroblastoma (SH-SY5Y) cell line and normal human epithelial hepatocytes, WRL-68 were obtained from the American Type Culture Collection (ATCC, Rockville, MD, United States). The cell lines were grown in Eagle's Minimum Essential Medium (EMEM, Corning, Mediatech, Manassas, VA, United States) supplemented with 10% fetal bovine serum (FBS, Gibco®, NY, United States) and 1% antibiotic penicillin (100 U/ml)/streptomycin (100 μ g/ml) (Gibco®, NY, United States). The cells were maintained at 37°C in a humidified incubator with 5% CO₂.

Preparation of Curcumin Analog (MS13) and Curcumin

MS13 or 1,5-bis(4-hydroxy-3-methoxyphenyl)-1,4-pentadiene-3-one was synthesized by coupling ketone with aldehyde in the ratio of 1:2, via base-catalyzed aldol condensation (Hosoya et al., 2012). Curcumin was purchased from commercial sources (Sigma Aldrich, St. Louis, MA, United States). Both MS13 and curcumin were dissolved in dimethyl sulfoxide (DMSO, Sigma



Aldrich, St. Louis, MA, United States) into 50 mM stock solution. The chemical structure of MS13 and curcumin are shown in **Figure 1**.

Cytotoxicity and Anti-Proliferative Assay

The cytotoxicity and anti-proliferative assay were performed using the MTT assay described by Mosmann (Mosmann, 2000) with slight modifications. U-87 MG, SH-SY5Y, and WRL-68 cells were seeded in 96 flat-bottomed tissue culture plate (Nunc™, Roskilde, Denmark) at seeding concentrations of 8×10^4 cells/ml and 10×10^4 cells/ml, respectively. The plates were incubated in a humidified incubator with 5% CO₂ at 37°C for 24 h to allow the cells to attach to the bottom of the wells. Subsequently, the media were aspirated out and replaced with 100 μl of MS13 or curcumin at their respective concentrations, i.e., 1.5625, 3.125, 6.25, 12.5, 25, 50, and 100 μM. Curcumin serves as positive control, while 0.2% DMSO serves as a negative control. The cells were treated for 72 h for dose-dependent cytotoxicity assay and 24, 48, and 72 h for dose- and time-dependent anti-proliferative assay. Following each treatment, the media containing the compounds were aspirated followed by the addition of 100 μl of 0.5 mg/ml of [3-(4,5-dimethylthiazol-2-yl)-2,5-diphenyltetrazolium bromide] (MTT). After 4 h, the MTT solution in each well was removed, and 100 μl of DMSO was added to solubilize the purple-colored formazan product. The absorbance was read at 570 and 640 nm using a microplate reader (BioTek EON™ Microplate Spectrophotometers, Fisher Scientific, United States). The absorbance reading was corrected to background absorbance, and average reading was taken from three independent experiments. The cell viability in percentage was calculated as follows:

$$\text{Cell viability (\%)} = \frac{\text{Average absorbance of treated cells}}{\text{Average absorbance of untreated cells (control)}} \times 100\% \quad (1)$$

The results were analyzed using GraphPad Prism version 8.0.2 for Windows (GraphPad Software, La Jolla, CA, United States). The half-maximal concentration (EC₅₀) for each biological replicate was determined using log-response curve constructed. Overall EC₅₀ was calculated from the average EC₅₀ of three independent biological replicates.

Selective Index

The selective index (SI) is the degree of selectivity of the compound tested against cancerous cells, in which values larger

than “100” indicates the compound is selective toward cancerous cells and confers minimal toxicity in normal non-malignant cells. It was calculated as follows:

$$\text{Selective index} = \frac{\text{EC}_{50} \text{ of WRL} - 68}{\text{EC}_{50} \text{ of U} - 87 \text{ MG/SH} - \text{SY5Y}} \times 100\% \quad (2)$$

Caspase-3 Colorimetric Assay

The caspase-3 activity in U-87 MG and SH-SY5Y cells upon exposure to MS13 was examined using RayBiotech® Caspase-3 Colorimetric Assay Kit #68Cl-Casp3-S100 (RayBiotech®, Inc., United States). The experiment was performed according to the instructions as described by the manufacturer. First, the cells were seeded in 75-cm² tissue culture flasks (SPL Life Sciences, South Korea) and treated with MS13 at two concentrations, i.e., $1 \times \text{EC}_{50}$ and $2 \times \text{EC}_{50}$ for three time points, i.e., 24, 48, and 72 h. Uninduced control cells were treated with 0.2% DMSO. Following each treatment, the cells were collected and lysed with 50 μl of chilled lysis buffer. The cell suspension was centrifuged, and cell lysate was collected. The protein concentration in the cell lysate was then quantified using the Pierce™ BCA Protein Assay Kit (Thermo Scientific, Pierce Biotechnology, Rockford, IL, United States). A similar protein amount, i.e., 200 μg was used for each treatment condition during the quantification of caspase-3 activity. A total of three independent experiments were performed, and each sample was quantified twice. The fold-change caspase-3 activity was calculated as follows:

$$\text{Fold-change of caspase-3 activity} = \frac{\text{Absorbance of MS13 induced samples at 405 nm}}{\text{Absorbance of uninduced control at 405 nm}} \quad (3)$$

Bcl-2 Concentration Colorimetric Assay

The bcl-2 concentration in U-87 MG and SH-SY5Y cells upon exposure to MS13 was examined using Invitrogen bcl-2 ELISA kit #BMS244-3 (Thermo Fisher Scientific, Rockford, IL, United States). The experiment was performed as described by the manufacturer. The cells were first seeded and treated in a similar manner described in the *Caspase-3 Colorimetric Assay* section. Upon exposure to each treatment condition, the cells were collected and lysed using the $1 \times$ lysis buffer provided. The cell suspension was incubated for 60 min at room temperature with gentle shaking. Subsequently, the cell lysate was collected, and the protein concentration was quantified using the Pierce™ BCA Protein Assay Kit. For each condition, 20 μl of the sample with a protein amount of 200 μg was used for the quantification

of bcl-2 concentration. A total of three independent experiments were performed, and the bcl-2 concentration of each sample was quantified twice.

Statistical Analysis

All experiments were conducted in triplicates. The EC₅₀ was reported as the mean ± standard error of the mean (SEM) from three biological replicates. Comparison between the datasets was performed using two-way analysis of variance (ANOVA). All statistical analyses were performed using GraphPad Prism version 8.1.2 for Windows (GraphPad Software, La Jolla, CA, United States).

Proteomic Analysis

MS13 Treatment and Cell Lysis

U-87 MG and SH-SY5Y cells were seeded in 75-cm² tissue culture flasks and exposed to 14 and 10 μM of MS13 (treatment group), respectively, to examine the differential protein expression profile. The cells in the control group were treated with 0.2% DMSO. The MS13 treatment period for U-87 MG and SH-SY5Y cells were 24 and 48 h, respectively. A total of three independent experiments were performed. Following treatment, the media were decanted, and the cells were collected, washed twice with cold 1× phosphate buffer saline (PBS, Corning®, Mediatech, Manassas, VA, United States) and lysed with 100 μl of RIPA buffer (Pierce Biotechnology, Thermo Fisher Scientific, Rockford, IL, United States) containing 1× phosphatase and protease inhibitor cocktail (Pierce Biotechnology, Thermo Fisher Scientific, Rockford, IL, United States). The cell suspension was homogenized using ultrasonic cell crusher (Scientz, China), and the cell pellet was spun down using a refrigerated centrifuge (Centrifuge 5424 R, Eppendorf, Germany) at 20,000 rpm, 4°C for 15 min. Subsequently, the cell lysate was collected and measured for its protein concentration using the PierceTM BCA Protein Assay Kit.

In-Solution Digestion

At 1 mg/ml, 60 μg of protein sample collected from each condition was subjected to in-solution digestion. Briefly, 25 μl of 100 mM ammonium bicarbonate (ABC, EMD Millipore, Germany), 25 μl of tetrafluoroethylene (TFE), and 1 μl of 200 mM dithiothreitol (DTT, EMD Millipore, Germany) were added to each protein sample. The sample mixture was vortexed briefly and heated at 90°C. After 1 h, the sample was left to cool until room temperature, followed by the addition of 4 μl of 200 mM iodoacetamide (IAM) (GE Healthcare, United Kingdom) to the mixture. The sample was incubated in the dark at room temperature for 1 h. One microliter of DTT was then added to the sample mixture, vortexed to mix well, and incubated in the dark at room temperature for another hour to quench excess IAM present in the sample mixture. After that, dilution of the sample mixture was performed by adding 300 μl of MilliQ water and 100 μl of ABC. Trypsin (Pierce Trypsin Protease, MS Grade, Thermo Fisher Scientific, Rockford, IL, United States) was then added in a protein:substrate ratio of 1:20, and the samples were incubated at 37°C for 24 h. Last, 1 μl of formic acid was added to stop the trypsin reaction.

The sample was then dried using centrifugal evaporator CVE-3100 (Eyela, Japan) and desalted through a C18 spin column (Pierce Biotechnology, Thermo Fisher Scientific, Rockford, IL, United States) as described in the manufacturer's protocol.

Liquid Chromatography Tandem Mass Spectrometry (LCMS/MS) Analysis

The dried, desalted peptide samples were reconstituted with 10 μl of 0.1% formic acid prior to being analyzed on nano-ESI-QTOF (Agilent, 65000 iFunnel Q-TOF LC/MS) equipped with Agilent Large Capacity Chip (G4240-62010 300Å-C18) that was equilibrated with 0.1% formic acid (solution A). One microliter of peptide sample was injected and eluted from the column at a flow rate of 500 nl/min with an increasing 5–70% of solution B, i.e., acetonitrile in water with 0.1% formic acid for 40 min. The polarity was set as positive, the capillary voltage at 1,900 V, and fragmenter voltage at 360 V. The drying gas flowed through the column at 325°C with a flow rate of 5.0 L/min. The spectra were then acquired in auto MS/MS mode in a mass range of 110–3,000 (m/z) for MS scan and 50–3,000 (m/z) for the MS/MS scan. The spectra were then analyzed using PEAKS X software (Bioinformatics Solutions Inc., Waterloo, ON, Canada).

Total Protein Identification and Label-Free Quantification

Protein identification in both control and treated samples were performed via automated *de novo* sequencing using PEAKS X software. The peptide spectra were matched against *in silico* digested *Homo sapiens* database downloaded from UniProt¹. A mass shift of 57.02 Da (carbamidomethylation), fragment mass tolerance of 0.1 Da, monoisotopic precursor, and false-discovery rate (FDR) less than 1.0% were set as the search criterion and trypsin as the digestion enzyme. LFQ was then performed on PEAKS Q module embedded in PEAKS X software. The mass error tolerance was set at 20 ppm, and retention time shift tolerance was set at 6.0 min. At FDR less than 1.0%, proteins that passed through significance (−10l gP) = 13 or equivalent to a *p*-value of less than 0.05, with at least one unique peptide, and a ratio less than 0.76 or more than 1.3 were selected as query terms for subsequent bioinformatic analysis. The ratio is defined as the protein intensity of treated sample vs. control sample.

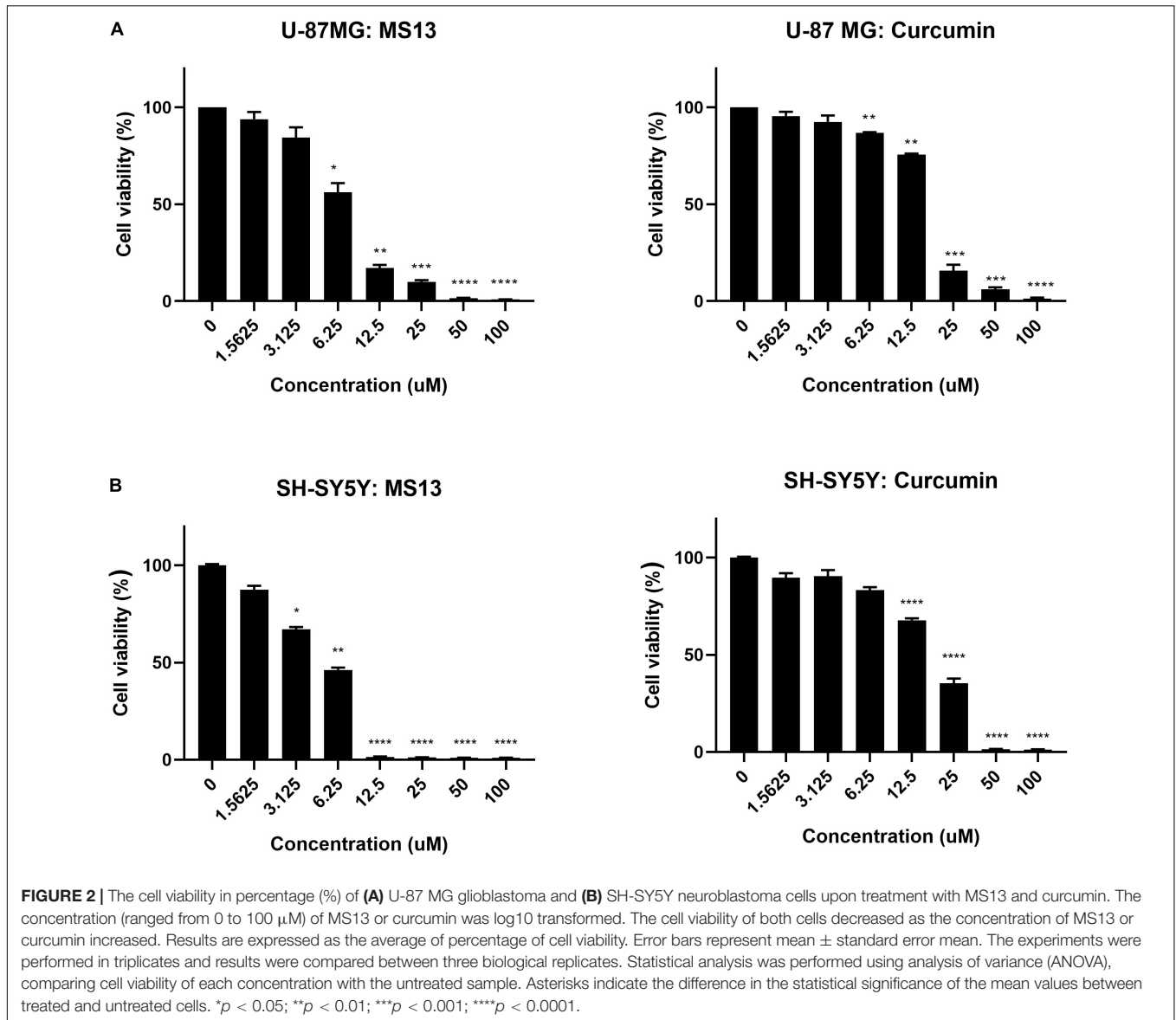
Bioinformatic Analysis

All DEPs obtained from the LFQ analysis were first classified into their respective PANTHER protein classes². Subsequently, statistical enrichment analysis for the biological process, molecular function, and cellular component of the DEP against the gene ontology (GO) consortium database³ was performed by submitting the DEPs list as query terms into BiNGO plugin (3.0.3) in Cytoscape (3.7.2) environment. The enriched GO terms were filtered from

¹<https://www.uniprot.org/>

²<http://www.pantherdb.org/>

³<http://geneontology.org/>



a *p*-value < 0.05 as the statistically significant cutoff upon the right-sided hypergeometric multiple correction testing with Benjamini–Hochberg option. The protein–protein interaction (PPI) network of all DEPs was then constructed from STRING (Search Tool for the Retrieval of Interacting Genes/Proteins)⁴, which maps the DEPs against the *Homo sapiens* database at high confidence score (0.70). To further identify highly connected protein clusters within the network, k-means clustering analysis was performed. Last, the DEPs identified were mapped to the reactome pathways⁵, in which overrepresentation test at FDR < 0.05 as the criterion was performed to select the associated enriched reactome pathways.

⁴<https://string-db.org/>

⁵<https://reactome.org/>

RESULTS

Determination of Cytotoxicity of MS13 in U-87 MG and SH-SY5Y Cells Using MTT Assay

The cytotoxicity of MS13 against human glioblastoma U-87 MG and SH-SY5Y cells were assessed by examining the cell viability at 72 h. Our results showed that MS13 induced a potent dose-dependent cytotoxic effect on U-87 MG and SH-SY5Y cells (Figure 2). Table 1 depicted a comparison of the EC₅₀ value of MS13 and curcumin on both SH-SY5Y cells. With an EC₅₀ value of approximately 1.4 times lower (U-87 MG: 6.78 ± 1.04 μM; SH-SY5Y: 4.72 ± 1.05 μM), MS13 was more potent toward SH-SY5Y cells than that of U-87 MG cells (*p* < 0.05). The EC₅₀ value of curcumin against both cell lines was about 2.5–3.5 times higher than that of MS13 (U-87 MG: 16.39 ±

TABLE 1 | Half maximal effective concentration (EC_{50}) of MS13 and curcumin against U-87 MG, SH-SY5Y and WRL-68 cells, and their respective selective index.

Compound	EC_{50} (mean \pm SEM) (μ M) ¹			Selective index (SI)	
	U-87 MG	SH-SY5Y	WRL-68	U-87 MG	SH-SY5Y
MS13	6.78 \pm 1.04	4.72 \pm 1.05	12.81 \pm 1.10	189	271
Curcumin	16.39 \pm 1.04	16.52 \pm 1.07	29.51 \pm 1.11	180	179

¹ EC_{50} values are presented as mean \pm standard error mean from three biological replicates.

1.04 μ M; SH-SY5Y: 16.52 \pm 1.05 μ M). Additionally, both MS13 and curcumin recorded an SI value of higher than 100, indicating that these compounds are selective toward human glioblastoma and neuroblastoma cells with minimal toxicity toward human normal cells (Table 1).

Determination of Anti-Proliferative Effect of MS13 in U-87 MG and SH-SY5Y Cells Using MTT Assay

The anti-proliferative effects of MS13 and curcumin were investigated by measuring the cell viability of U-87 MG cells upon exposure for 24, 48, and 72 h. As shown in Figure 3, MS13 demonstrated dose- and time-dependent anti-proliferative effects on U-87 MG and SH-SY5Y cells. By referring to Table 2, the EC_{50} value of MS13 in U-87 MG cells decreased significantly by about 50% ($p < 0.05$) as the treatment time increased from 24 to 48 h. More significant growth inhibition with a decrease in EC_{50} value to 6.78 μ M ($p < 0.01$) was observed when the incubation time increased further to 72 h. Similarly, a progressive reduction in EC_{50} value was observed in SH-SY5Y cells upon MS13 treatment following prolonged treatment time to 72 h. A significant reduction ($p < 0.01$) in EC_{50} value was also observed in these cells following MS13 treatment for 72 h. On the contrary, the cell viability for both U-87 MG and SH-SY5Y remained high following curcumin treatment. The EC_{50} of curcumin were approximately two to four times higher than that of MS13 at all three time-points.

Determination of Apoptosis Activity Using Caspase-3 and bcl-2 Colorimetric Assay

The caspase-3 activity and bcl-2 concentration in MS13-treated U-87 MG cells were quantified using colorimetric assays, and the cell morphology upon MS13 treatment is shown in Supplementary Figures 1, 2. Our result revealed a significant increase in caspase-3 activity when U-87 MG cells were exposed to 14 μ M MS13 for 24, 48, and 72 h but peaked at 48 h with a fold-change of 3.4 in a dose-dependent manner. However, no significant increase was noted following the treatment with 7 μ M MS13 for the same period (Figure 4A). On the other hand, the caspase-3 activity in SH-SY5Y cells increased significantly at fold-change 2.8 and peaked at 3.3 following treatment with 10 μ M of MS13 for 24 and 48 h, respectively (Figure 4B). No significant increase in the activity was noted in cells treated with

5 μ M of MS13 for 24 h, although the activity was found to increase significantly to a fold change of 2.4 as the treatment time prolonged to 48 h. Nevertheless, a decrease in caspase-3 activity was noted with a fold change of less than 1.5 after treatment with 5 or 10 μ M for 72 h.

Contrarily, the bcl-2 concentration in both U-87 MG and SH-SY5Y cells was found to decrease significantly upon exposure to MS13. In U-87 MG cells, reduction in bcl-2 was noted following treatment with 7 μ M, and the reduction was more prominent when treated with 14 μ M of MS13 for 24, 48, and 72 h (Figure 5A). Similarly, the bcl-2 concentration in SH-SY5Y cells reduced significantly following treatment with 5 μ M of MS13, and a greater reduction of bcl-2 concentration was observed when the concentration of MS13 was increased to 10 μ M and exposed for 24, 48, and 72 h (Figure 5B). These data suggest that MS13 induces apoptosis via caspase-3 and mitochondrial-dependent pathway in U-87 MG cells in a dose- and time-dependent manner.

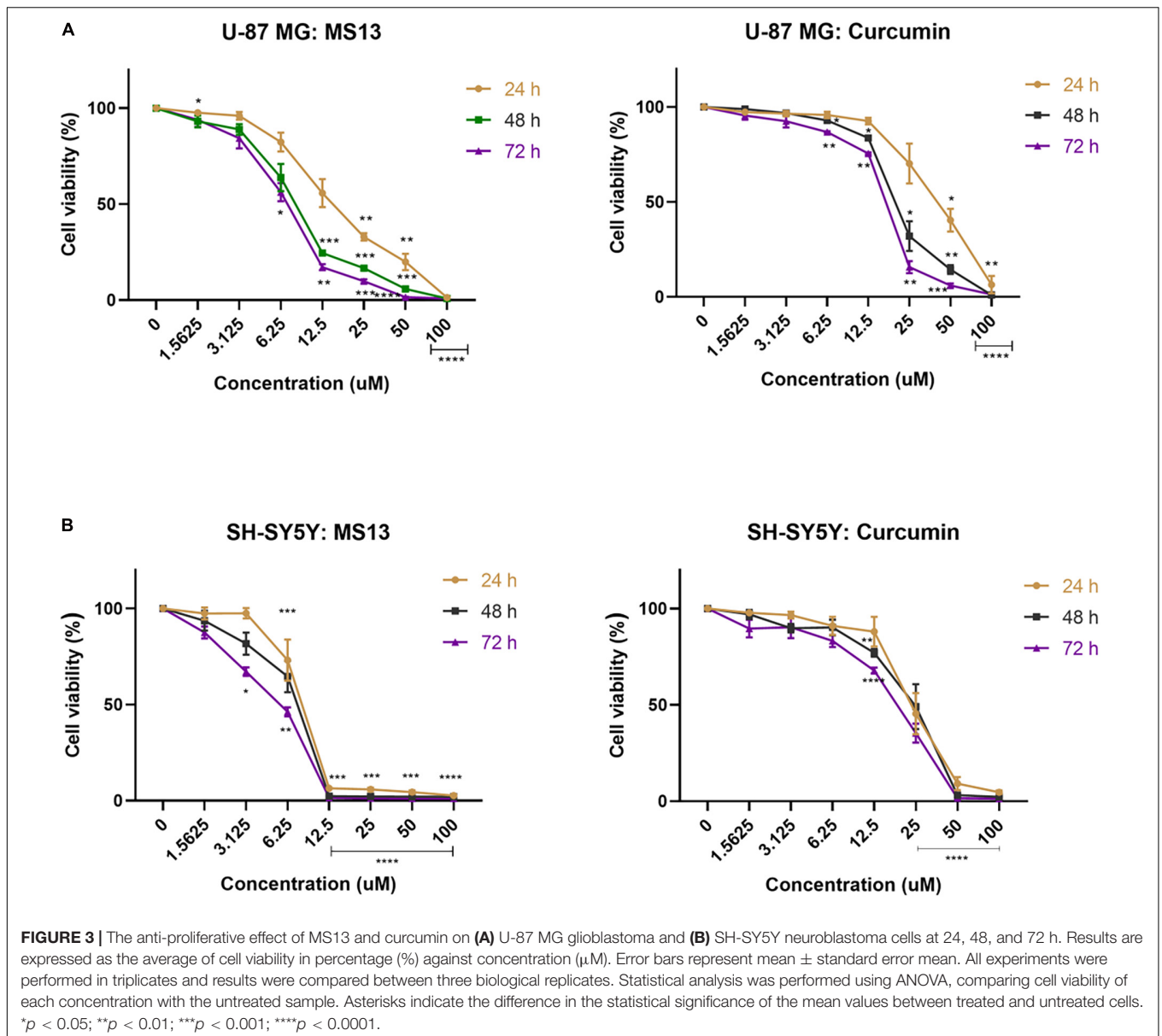
Analysis of DEPs in MS13-Treated U-87 MG and SH-SY5Y Cells via Shotgun Proteomic Approach

The differential protein expression profile in U-87 MG and SH-SY5Y cells following MS13 treatment was investigated via label-free shotgun proteomic approach. The optimum dosage and time selected for U-87 MG and SH-SY5Y cells were 14 μ M ($2 \times EC_{50}$) of MS13 for 24 h and 10 μ M ($2 \times EC_{50}$) of MS13 for 48 h, respectively. These parameters were selected based on the data analysis obtained from cytotoxicity, anti-proliferative, and apoptosis assays, whereby the cells were undergoing apoptosis with at least 50% cell viability upon exposure to these treatment conditions. A total of 406 and 349 proteins were identified in U-87 MG cells in the control and treatment group, respectively. Among these proteins, a total of 30 DEPs comprising of nine upregulated and 21 downregulated proteins were identified in MS13-treated U-87 MG cells. In SH-SY5Y cells, 437 and 435 proteins were determined in the control and treatment group, respectively, and 38 DEPs that comprise of seven upregulated and 31 downregulated proteins were identified.

Gene Ontology: Functional Annotation

The DEPs lists identified in U-87 MG and SH-SY5Y cells were uploaded to BiNGO plugin in Cytoscape for functional annotation analysis. The enriched GO terms in each functional category, namely, the molecular function, cellular component, and biological process were identified (Figure 6).

In U-87 MG cells, the GO terms “Nitric-oxide synthase regulator activity” (22.2%) ($p < 0.0001$) and “Unfolded protein binding” (33.3%) ($p < 0.001$) appeared to be the most significantly enriched GO terms among the upregulated proteins, while the “Translation elongation factor activity” (19%) ($p < 0.0001$), “Protein binding” (95.2%) ($p < 0.001$), and “Ribonucleoprotein binding” (14.2%) ($p < 0.001$) were the most significantly enriched GO terms among the downregulated proteins in the molecular function category (Figure 6B). On the



other hand, “Unfolded protein binding” (67.1%) ($p < 0.0001$), “ATPase activity” (28.5%) ($p < 0.0001$), and “TPR domain binding” (28.5%) ($p < 0.001$) were the most significantly enriched molecular function GO terms annotated by upregulated proteins in SH-SY5Y cells (Figure 6B). Although the majority of the downregulated proteins were associated with protein binding (76.6%), the association was not highly significant ($p < 0.05$).

Based on the cellular component category, the most significantly enriched GO term annotated by the upregulated proteins in U-87 MG cells was “Myosin complex” (22.2%) ($p < 0.01$). However, the majority of the downregulated proteins (90.4%) were associated with “Cytoplasm” and noted as the top most significantly enriched ($p < 0.001$) GO term, while all (100%) upregulated proteins in the SH-SY5Y cells were associated with “Cytoplasm” and “Membrane-bounded organelle,” whereas the

majority of the downregulated proteins (73.3%) were associated with “Cytoplasm.” Nonetheless, “Protein–DNA complex” (16.6%) ($p < 0.0001$) and “Cytoskeleton” (20.0%) ($p < 0.001$) were the two most significantly enriched cellular component GO terms annotated by downregulated proteins.

The most enriched biological process GO term among the upregulated proteins in U-87 MG cells was “Response to unfolded protein” (42.8%) ($p < 0.01$). However, the “Translational frameshifting” (14.2%) ($p < 0.0001$), “Regulation of apoptosis” (38.0%) ($p < 0.001$), and “Glycolysis” (14.2%) ($p < 0.001$) were the most significant GO terms identified among the downregulated proteins. Although all the downregulated proteins in this category were associated with “cellular process” (100%) and a large proportion with “metabolic process” (71.4%), the statistical analysis indicated the association was

TABLE 2 | Half maximal effective concentration (EC₅₀) of MS13 and curcumin against U-87 MG and SH-SY5Y cells at 24, 48, and 72 h.

Compound/cell line	EC ₅₀ (mean ± SEM) (μ.M) ¹		
	24 h	48 h	72 h
MS13			
U-87 MG	15.93 ± 1.06	8.13 ± 1.05*	6.78 ± 1.04**
SH-SY5Y	7.36 ± 1.05	6.84 ± 1.06	4.72 ± 1.05*
Curcumin			
U-87 MG	38.80 ± 1.06	20.45 ± 1.06*	16.39 ± 1.04
SH-SY5Y	22.54 ± 1.06	21.39 ± 1.08	16.52 ± 1.07

¹EC₅₀ values are presented as mean ± standard error mean from three biological replicates. **p* < 0.05; ***p* < 0.01.

not highly significant. Similarly, a majority of the upregulated proteins in SH-SY5Y cells were associated with “Response to unfolded protein” (83.3%) and “Protein folding” (66.6%), whereby these GO terms were highly significant (*p* < 0.0001). Additionally, “Chaperone-mediated protein complex assembly” (33.3%) (*p* < 0.001) was another highly significant biological process GO term annotated by these proteins. On the contrary, “Response to calcium ion” (13.3%) (*p* < 0.001), “Regulation of cytokinesis” (10.0%) (*p* < 0.001), and “Regulation of transporter activity” (10.0%) (*p* < 0.001) were highly significant enriched biological process GO terms annotated by downregulated proteins. Although majority of these proteins were associated with the cellular process (90.0%), the statistical analysis revealed that the association was not highly significant.

Protein Identification and Classification

The DEPs identified in MS13-treated U-87 MG and SH-SY5Y cells with a ratio of more than 1.3 and less than 0.76 were grouped as upregulated and downregulated proteins, respectively. These DEPs were then classified into their respective protein classes by mapping them into the PANTHER classification system. Nine of the DEPs, including heat shock protein HSP 90-alpha (HSP90AA1), HSP90AB1, tubulin beta chain (TUBB), glyceraldehyde 3-phosphate dehydrogenase (GAPDH), alpha-enolase (ENO1), histone H2AX (H2AFX), heterogenous nuclear ribonucleoprotein K (HNRNPK), eukaryotic translation initiation factor 5A-1 (EIF5A), and SET were commonly found in MS13-treated U-87 MG and SH-SY5Y cells.

By referring to **Supplementary Table 1**, the upregulated proteins identified in MS13-treated U-87 MG cells were grouped into four protein classes. The top protein classes were chaperone and cytoskeletal-binding protein, each comprised 44% (4/9) and 33% (3/9) of the upregulated proteins, while histone and metabolic enzyme comprised 11.1% (1/9) of the proteins. The downregulated proteins were classified into nine protein classes. The top protein class identified was the RNA-binding protein that comprised 23.8% (5/21) of the downregulated proteins followed by metabolic enzyme and chaperone, wherein each comprised 19.0% (4/21) of the proteins. The remaining of the protein classes grouped by downregulated proteins included histone and cytoskeletal protein, wherein each made up of 9.5% (2/21) of the proteins, and ribosomal protein, calcium-binding protein,

enzyme modulator, and cytoskeletal binding protein, wherein each constituted 4.8% (1/21) of the proteins.

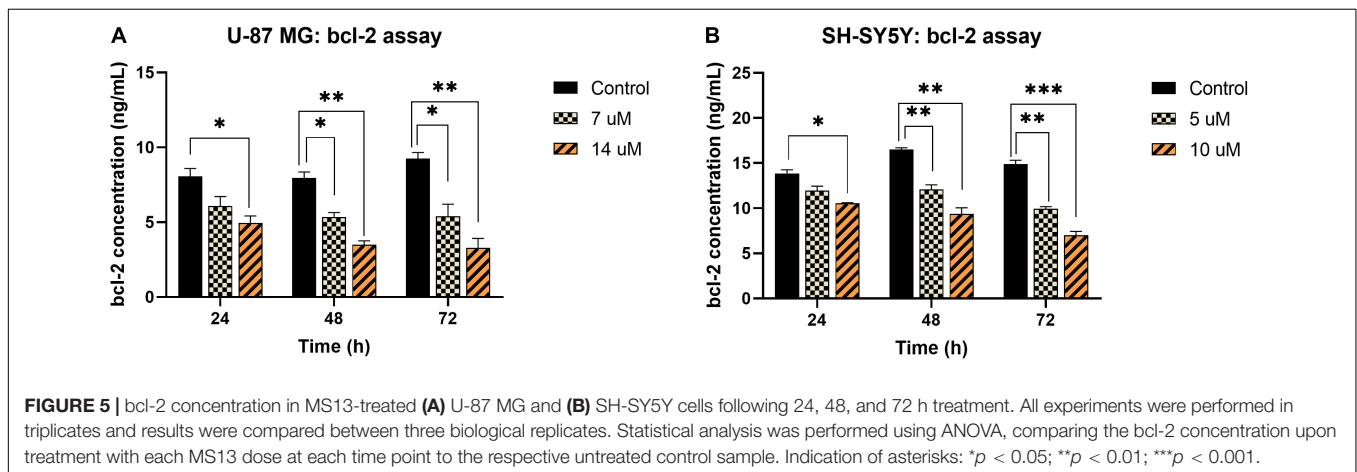
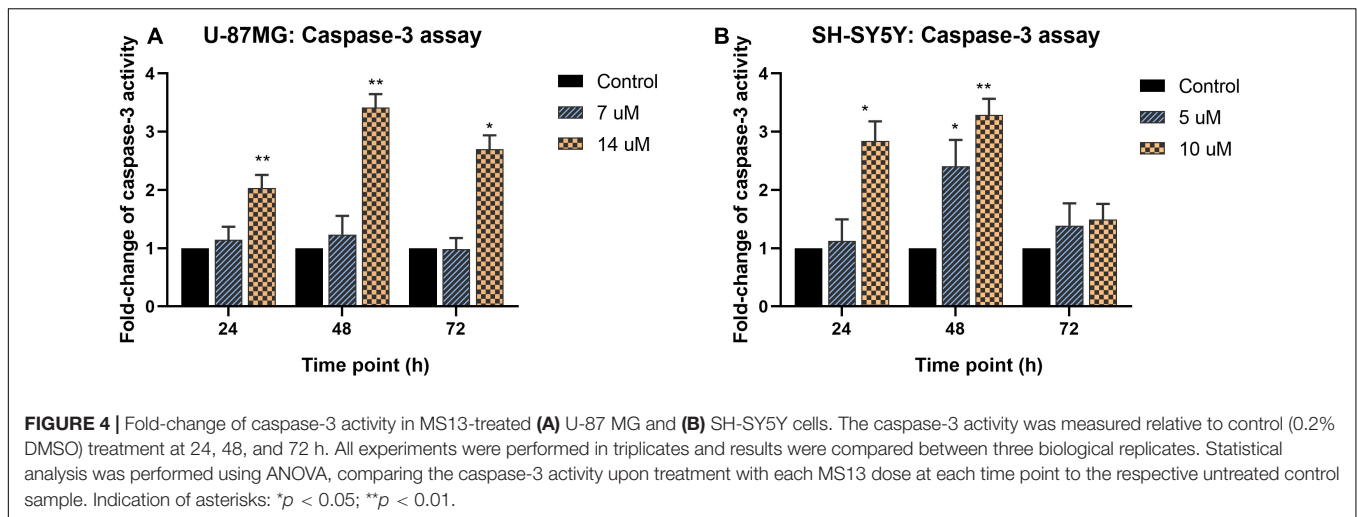
On the other hand, the upregulated proteins in MS13-treated SH-SY5Y cells were grouped into three protein classes (**Supplementary Table 2**). Chaperone was the top protein class, which comprised 71.4% (5/7) of the proteins. The remaining protein classes were metabolic enzymes and cytoskeletal-binding proteins, and each consisted 14.3% (1/7) of the upregulated proteins. A total of 31 downregulated proteins were determined and classified into 12 protein classes. The top protein classes were histones and cytoskeletal proteins that comprised 19.4% (6/31) of the downregulated proteins. This was followed by metabolic enzymes, RNA-binding protein, calcium-binding protein, and enzyme modulator, which comprised 16.1% (5/31), 12.9% (4/31), 9.7% (3/31), and 6.5% (2/31) of the proteins. However, 3.2% (1/31) of the downregulated proteins were ribosomal protein, cytoskeletal-binding protein, cell adhesion molecule, cation transporter, and chaperone.

Protein–Protein Interaction Network

The PPI network of all DEPs identified in MS13-treated U-87 MG (*p* = 2.64 × 10¹⁴) and SH-SY5Y (*p* = 1.84 × 10^{−14}) cells are presented in **Figures 7A,B**, respectively. A total of 30 nodes and 46 edges were identified in the PPI network of U-87 MG cells, while 38 nodes and 68 edges were found in SH-SY5Y cells. A significant interaction between DEPs with average local clustering of 0.663 and 0.604 for U-87 MG and SH-SY5Y cells, respectively, were determined. Both networks also revealed that the DEPs with similar functional roles were grouped into a cluster, and inter-cluster interactions were clearly displayed.

In MS13-treated U-87 MG cells, a total of six highly connected clusters were generated from k-means clustering analysis. Among the six clusters, clusters 1, 2, and 3 were highly connected. Cluster 1 was made up of RNA-binding proteins (e.g., EIF5A, EIF5A2, EIF5AL1, and EEF2) and ribosomal proteins (e.g., RPS13). Metabolic enzymes (e.g., ENO1, MDH2, GAPDH, TPI1, and PRDX1) and cytoskeletal protein (e.g., TUBB) made up Cluster 2. Chaperones including CALR, PDIA6, and heat shock proteins (e.g., HSP90AB1, HSP90AA1, HSP90B1, and HSPA5) made up cluster 3. Clusters 4, 5, and 6 each were made up of histones (e.g., HIST1H2BB, H2AFX, and HIST1H2BJ), 14-3-3 proteins (e.g., YWHAZ and YWHAQ), and cytoskeletal proteins (e.g., MYL12B, MYL12A, and TLN1). The remaining un-clustered proteins were ANXA1, PFN1, FLNC, SET, and HNRNPK.

In MS13-treated SH-SY5Y cells, a total of seven clusters were made up of DEPs with similar functional roles identified. The first cluster was made up of histones (e.g., H2AFZ, H2AFV, HIST1H4A, HIST1H2AA, and H2AFX). Cluster 2 consists of cytoskeletal proteins (e.g., ACTB, ACTG1, MYH9, TUBB2B, and CDC42) and metabolic enzymes (e.g., PGK1 and GAPDH), while Cluster 3 was made up of metabolic enzymes (e.g., ENO1 and P4HB) and cell adhesion molecules (e.g., LGALS1). Cluster 4 was made up of RNA-binding proteins (EIF5A) and ribosomal proteins (RPLP2). Clusters 5 and 6 each consisted of calmodulins



(CALM1, CALM2, and CALM3) and RNA-binding proteins (HNRNPK, HNRNPU, and HNRNPK). Chaperones (e.g., HSPB1, HSP90AB1, HSP90AA1, HSPD1, HSPE1, and YWHAE), cation transporters (e.g., ATP5B), and cytoskeletal proteins (e.g., TUBB) made up Cluster 7. The remaining unclustered proteins were HIST1H1B, STMN1, SET, PRDX6, VIM, LMNA, and ISOC1.

Pathway Analysis

All DEPs identified in MS13-treated U-87 MG and SH-SY5Y cells were then mapped into the reactome pathway database to identify the possible pathways modulated by MS13. An overrepresentation analysis was performed. “Glycolysis” and “Post-translational protein modification” were the two common pathways identified in both U-87 MG and SH-SY5Y cells. The rest of the top enriched pathways identified in U-87 MG cells were “G2/M DNA damage checkpoints,” “Axon guidance,” and “Intrinsic pathway for apoptosis,” while for SH-SY5Y cells, “Rho GTPase-activated IQGAPs,” “Cellular responses to stress,” and “Apoptotic execution phase” pathways were identified. The DEPs mapped to each pathway are tabulated in **Table 3**.

DISCUSSION

The present study showed that the viability of U-87 MG and SH-SY5Y cells decreased as the concentration of curcumin and MS13 increased. Notably, MS13 induced more potent cytotoxicity and anti-proliferative effects, with an EC_{50} value approximately 2.4- and 3.5-fold lower than that of curcumin in U-87 MG and SH-SY5Y cells, respectively. Additionally, the reduction in cell viability follows a dose- and time-dependent manner. The selectivity of MS13 against cancerous cells was verified by comparing the EC_{50} of MS13 on cancerous cells against normal hepatocytes. A higher SI value depicted by MS13 further implies that MS13 is not only being a more toxic compound, but it is also selective toward cancerous cells compared with curcumin. However, to further compare the selectivity of MS13 between brain cancerous and normal cells, the cytotoxicity effect of MS13 on normal glial and neuronal cells warrants further investigation in the future. The chemical modification in the central spacer region of curcumin may account for the enhanced cytotoxicity and anti-proliferative effects as displayed by MS13. Liang et al. (2009) revealed that the weak pharmacokinetic profiles of curcumin were due to the high susceptibility of OH-

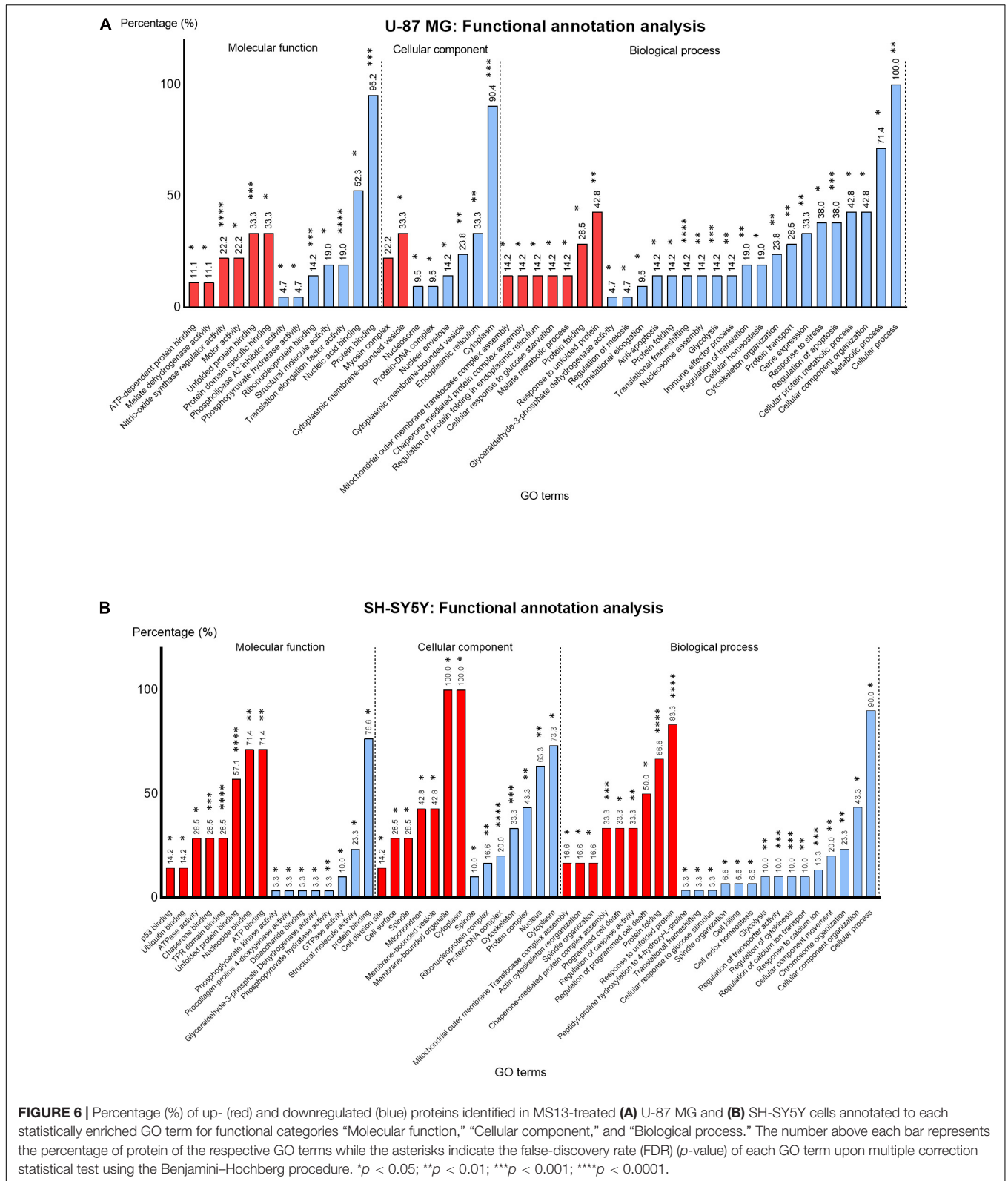


FIGURE 6 | Percentage (%) of up- (red) and downregulated (blue) proteins identified in MS13-treated (A) U-87 MG and (B) SH-SY5Y cells annotated to each statistically enriched GO term for functional categories “Molecular function,” “Cellular component,” and “Biological process.” The number above each bar represents the percentage of protein of the respective GO terms while the asterisks indicate the false-discovery rate (FDR) (*p*-value) of each GO term upon multiple correction statistical test using the Benjamini–Hochberg procedure. **p* < 0.05; ***p* < 0.01; ****p* < 0.001; *****p* < 0.0001.

in the central spacer β-diketone moiety toward nucleophilic attack. The curcumin analog that lacks the β-diketone moiety is more stable and often exhibits enhanced biological activities

than those of curcumin (Liang et al., 2009). Additionally, MS13 also demonstrated a higher degree of cytotoxicity with a lower EC₅₀ value compared with curcumin on several cancer cells,

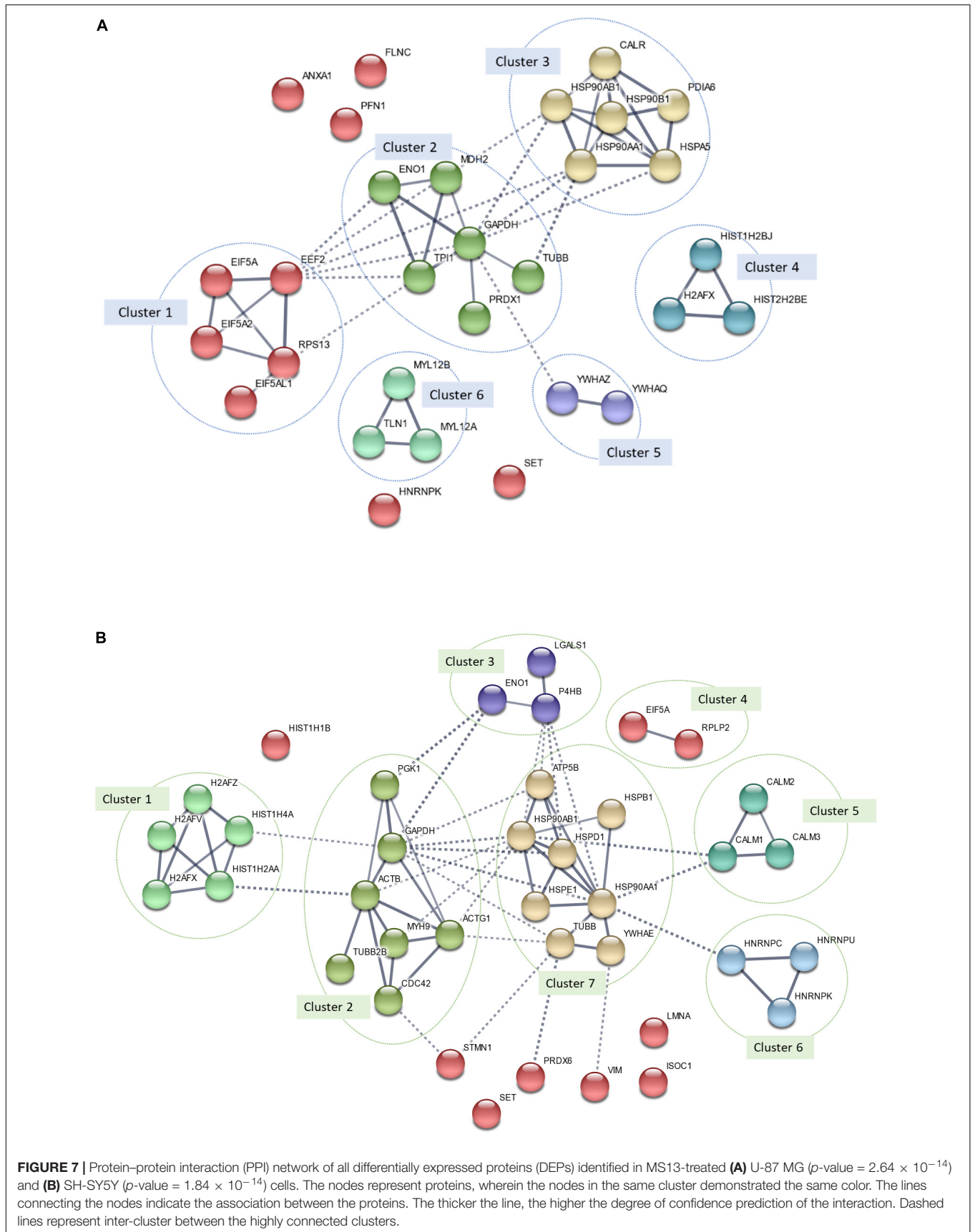


TABLE 3 | Enriched reactome pathways mapped by all DEPs identified in MS13-treated U-87 MG and SH-SY5Y cells.

Pathway ID	Pathway name	Protein ¹	FDR ²
U-87 MG			
R-HSA-69481	G2/M DNA damage checkpoints	H2AFX*; YWHAQ; HIST2H2BE; HIST1H2BJ; YWHAZ	1.01 × 10 ⁻³
R-HSA-422475	Axon guidance	HSP90AA1*; HSP90AB1*; MYL12B; MYL12A; PFN1; TLN1	2.36 × 10 ⁻³
R-HSA-70171	Glycolysis	ENO1*; GAPDH*; TPI1	3.59 × 10 ⁻³
R-HSA-109606	Intrinsic Pathway for Apoptosis	YWHAQ; YWHAZ	1.79 × 10 ⁻²
R-HSA-597592	Post-translational protein modification	HIST2H2BE; HIST1H2BJ; EIF5A2; EEF2; PDIA6; EIF5A*; HSP90B1; HNRNPK*; CALR	1.97 × 10 ⁻²
SH-SY5Y			
R-HSA-194315	Rho GTPase activates IQGAPs	TUBB2B; TUBB*; ACTB; ACTG1; CALM1; CDC42	1.24 × 10 ⁻⁵
R-HSA-2262752	Cellular responses to stress	HSP90AA1*; HSP90AB1*; HIST1H4A; HIST1H1B; H2AFX*; H2AFZ; H2AFV; PRDX6; P4HB; YWHAZ	1.87 × 10 ⁻⁵
R-HSA-75153	Apoptotic execution phase	VIM; LMNA; HIST1H1B	3.50 × 10 ⁻³
R-HSA-70171	Glycolysis	ENO1*; GAPDH*; PGK1	8.29 × 10 ⁻³
R-HSA-392499	Post-translational protein modification	EIF5A*; HNRNPC; HNRNPK*; HIST1H4A; HIST1H2AA; TUBB2B; P4HB; CALM1	4.54 × 10 ⁻²

¹Proteins in blue and purple represents up- and downregulated proteins, respectively.

²FDR, false discovery rate, corrected using Benjamini–Hochberg multiple testing procedure.

*Common differentially expressed proteins (DEPs) identified in both U-87 MG and SH-SY5Y cells.

including nasopharyngeal (Liang et al., 2009), colorectal (Cen et al., 2009; Liang et al., 2009), prostate (Citalingam et al., 2015), cervical (Paulraj et al., 2015), and gastric (Yoshida et al., 2018) cancer cells. The present findings are consistent with previous studies indicating that the removal of the β-diketone moiety may yield compounds that exhibit improved cytotoxicity and anti-proliferative effects over its parent compound.

The cytotoxicity and anti-proliferative effects induced by MS13 were more potent in neuroblastoma SH-SY5Y cells compared with human glioblastoma U-87 MG cells. Glioblastoma originates from astrocytes, while neuroblastoma arises from neuroblasts. Kim et al. (2015) have reported that U-87 MG cells adopted a specific carbohydrate metabolism and allowed these cells to possess a higher metabolic capacity; thus, they divide more rapidly, compared with SH-SY5Y cells. Additionally, the molecular disparity between U-87 MG and SH-SY5Y cells may also account for the difference in sensitivity toward MS13 treatment, wherein the former cells documented chromosomal deletions (Miyakawa et al., 2000), while the latter has been reported to harbor a complete set of chromosomes (Yusuf et al., 2013). Collectively, it is suggested that both biological and molecular characteristics are responsible for the sensitivity of U-87 MG and SH-SY5Y cells toward MS13 treatment, with a therapeutic advantage against neuroblastoma cells by MS13.

Apoptosis is a preferable means exploited by anti-neoplastic agents during chemotherapy as it removes potentially harmful cells without causing extensive inflammatory-associated damage in the body. In the present study, caspase-3 activity and concentration of bcl-2 were determined in U-87 MG and SH-SY5Y cells following treatment with 1 × EC₅₀ (U-87 MG: 7 μM; SH-SY5Y: 5 μM) and 2 × EC₅₀ (U-87 MG: 14 μM; SH-SY5Y: 10 μM) of MS13 at three-time points, 24, 48, and 72 h. Caspase-3, which plays a critical role in executing apoptosis, is an effector molecule activated by caspase-8, -9, and -10. Given that caspase-3 regulates the occurrence of the downstream biochemical and morphological hallmarks

(Boland et al., 2013), it is introduced as a potential druggable molecular target for the chemotherapeutic agent. Our present findings revealed that caspase-3 activity increased in a dose-dependent manner and peaked at 48 h in both MS13-treated U-87 MG and SH-SY5Y cells. Supportively, FLLL-11, which has an identical chemical structure as MS13 and diarylpentanoid B19, induced apoptosis in human colorectal cancer (Cen et al., 2009) and ovarian cancer (HO8910) (Qu et al., 2013) cells via activation of caspase-3, respectively. Bcl-2- is an anti-apoptotic protein in the BCL-2 family that regulates the mitochondrial-dependent apoptosis pathway via the inhibition of membrane permeabilization activity and suppression of the release of cytochrome c (Kalkavan and Green, 2018). Given the positive correlation between bcl-2 overexpression and tumorigenesis, compounds that downregulate bcl-2 may confer a therapeutic advantage in treating cancers (Adams and Cory, 2018). We demonstrated a progressive reduction in bcl-2 concentration in both U-87 MG and SH-SY5Y cells upon exposure to MS13, and the reduction is in a dose- and time-dependent manner. Earlier studies had also noted similar observations when melanoma cells were treated with diarylpentanoid (DM-1) (Faião-Flores et al., 2013) and hepatocellular carcinoma cells with EF24 (Liu et al., 2012). These findings suggest that MS13 induces mitochondrial-dependent apoptosis in both U-87 MG and SH-SY5Y cells.

To date, no previous studies have been conducted to investigate the anti-cancer effects of MS13 via the shotgun proteomics approach. Therefore, the large-scale proteomics analysis performed in our current study shed a light on the protein expression profile of U-87 MG and SH-SY5Y cells following MS13 treatment. Enrichment analysis of these DEPs using functional annotation demonstrated several most significantly enriched GO terms in the cellular component, biological process, and molecular function categories. The most significantly enriched GO terms commonly identified in both cell lines were the unfolded protein binding categorized under molecular function, and response to unfolded protein and

glycolysis under the biological process. Notably, GO terms such as cytoplasm, translational frameshifting, regulation of apoptosis, nitric oxide synthase regulator activity, protein binding, translation elongation factor activity, and ribonucleoprotein binding were found highly significantly enriched in U-87 MG cells; while cytoskeleton and protein-DNA complex, ATPase activity and TPR domain binding, protein folding, chaperone-mediated protein complex assembly, response to calcium ion, regulation of cytokinesis, and regulation of transporter activity were observed in SH-SY5Y cells. These findings suggest that MS13 induces cytotoxicity, anti-proliferation, and apoptosis in U-87 MG and SH-SY5Y cells through DEPs associated with cellular and metabolic processes, cellular responses, transcriptional and translational regulation, induction of cellular stress, and transporter activity.

We further investigate the interaction of all DEPs identified in MS13-treated U-87 MG and SH-SY5Y cells by performing PPI network analysis, which revealed the functional network. Furthermore, integration of DEPs from PPI network analysis with the top five reactome pathways of both cell lines revealed that proteins in the clusters also mapped into the pathways underscores the importance of these pathways in determining the anti-cancer effects of MS13 in U-87 MG and SH-SY5Y cells. The common DEPs that were mapped in the pathways include GAPDH, ENO1, HSP90AA1, heat shock protein HSP 90-beta (HSP90BAB1), EIF5A, HNRNPK, and H2AFX. Additionally, TUBB was the common DEPs that mapped only to the enriched pathway in SH-SY5Y but not U-87 MG cells, while Protein SET (SET) did not map into any of the enriched pathways. We will focus on the biological significance of these proteins in the respective clusters and associated pathways.

Glyceraldehyde 3-phosphate dehydrogenase and ENO1, as mutually downregulated proteins identified in both U-87 MG and SH-SY5Y cells, were mapped to one of the mutual pathways “Glycolysis” for both cell lines. The Warburg hypothesis indicated aerobic glycolysis as one of the core metabolic pathways employed by cancer cells to generate energy (Warburg, 1956). Given this hypothesis, targeting the molecules along the glycolytic pathway confers a therapeutic advantage in treating cancer cells by starving these cells to death. GAPDH catalyzes the conversion of glyceraldehyde-3-phosphate (GAP) to 1,3-bisphosphoglycerate (1,3BP) and ENO1 dehydrates 2 phosphoglycerate (2PG) to form phosphoenolpyruvate (PEP). These interconnected glycolytic proteins catalyze the conversion of glucose to generate ATP, NADH, and pyruvate molecules to support the high load of anabolic reaction in cells. Overexpression of these proteins in the secretome of a glioblastoma cell line was associated with the progression of glioblastoma (Gupta et al., 2013). Li et al. (2019) also showed that the growth and the progression of SH-SY5Y cells were significantly reduced following treatment with glycolysis inhibitory peptide. Altogether, the findings imply that MS13 may demonstrate its anti-cancer effects in U-87 MG and SH-SY5Y cells by downregulating GAPDH and ENO1, which disrupts the glycolytic pathway and subsequently results in the reduction of energy production and inhibition of cell proliferation.

The heat shock proteins, HSP90AA1 and HSP90AB1 were found upregulated in both U-87MG and SH-SY5Y cells and mapped to “Axon guidance” and “Cellular responses to stress” pathways, respectively. The key functional role of these cytoplasmic chaperones is to regulate protein homeostasis by maintaining the proteome in a folded and functional state (Calderwood and Murshid, 2017). Hence, the upregulation of heat shock proteins as inducible chaperones is expected as the proteolytic and oxidative insults accumulate. HSP90AA1 and HSP90AB1 are involved in the axon guidance pathway, via an association with the semaphorins and their signaling mechanism. The axon guidance pathway regulates the neural development and migration, wherein semaphorins are one of the protein families that finetune the morphology and motility of various types of cells including those associated with the nervous system (Chedotal et al., 2005). Additionally, both HSP90AA1 and HSP90AB1 also regulate the LIM kinase (LIMK) protein dimerization and prevent the binding of phosphorylated cofilin to the actin molecules (Li et al., 2006). Hence, the upregulation of HSP90AA1 and HSP90BB1 in the current study indicates the ability of MS13 to induce environmental stress and inhibit the actin polymerization activity, leading to the disruption of the cytoskeletal remodeling process. The findings suggest that these proteins may inhibit cell migration, activate cytoprotective measure upon exposure to an increase oxidative or proteolytic stress as induced by MS13 and apoptosis in U-87 MG and SH-SY5Y cells.

The RNA-binding proteins, EIF5A and HNRNPK, were downregulated in U-87 MG and SH-SY5Y cells that mapped to “Post-translational protein modification,” a pathway that significantly imparts a dynamic complexity in proteins, leading to a diverse functional role of the proteins (Krueger and Srivastava, 2006). The EIF5A is a translational factor that is involved in polypeptide chain elongation, while the isoform of EIF5A-EIF5A2- was identified exclusively in U-87 MG cells and is also downregulated in this pathway. Both proteins are activated upon hypusination, a two-step enzymatic post-translational modification process that transform the lysine residue of the translation factors to hypusine and is involved in the regulation of cell growth and proliferation (Mathews and Hershey, 2015). The overexpression of both isoforms was associated with poor prognosis of glioblastoma (Preukschas et al., 2012). The spermidine and deoxyhypusine synthase (DHPS) inhibitor, GC7, inhibits activation of EIF5A and induces apoptosis of neuroblastoma cells via the regulation of the p21/Rb signaling axis (Bandino et al., 2014). Consistently, the knockdown of EIF5A2 inhibits the migration and invasion of non-small cell lung cancer cells (Chen et al., 2018). On the other hand, the HNRNPK regulates activities associated with RNA metabolism, including pre-mRNA processing and mRNA nucleo-cytoplasmic transportation. HNRNPs promote cell proliferation and metastasis by binding to oncogenes, such as *c-myc* at their promoter region (Kim et al., 2003). The overexpression of HNRNPK was associated with neuroblastoma progression (Li et al., 2018), while downregulation of HNRNPK repressed glioblastoma cell proliferation and induced apoptosis (Wu et al., 2020). Collectively, our current finding suggests that

downregulation of EIF5A and HNRNPK by MS13 may inhibit cell proliferation and migration as well as induce apoptosis in glioblastoma and neuroblastoma cells.

Histones are essential in packaging the DNA double helix into nucleosomes. H1 proteins are linkers that stabilize histone octamers, i.e., H2, H3, and H4 (Chikhirzhina et al., 2018). The core histone variant, H2AFX, was identified as one of the common DEPs in both cells, and was up- and downregulated in U-87 MG and SH-SY5Y cells, respectively. This protein was mapped to different pathways, “G2/M DNA damage checkpoints” and “Cellular responses to stress” for U-87 MG and SH-SY5Y cells, respectively. The H2AFX is a DNA double-stranded break response protein that accumulates and activates the CHEK2 protein via auto-phosphorylation at the G2/M DNA damage checkpoint. The activated CHEK2 protein inhibits CDC25C phosphatase, stabilizes the p53 protein, and halts the cell cycle progression. Liu et al. (2007) reported that H2AFX may serve as a tumor suppressor protein, and its upregulation sensitizes the gastrointestinal stromal tumor cells to imatinib chemotherapeutic drug treatment. Nevertheless, downregulation of H2AFX may also indicate genomic instability in cells exposed to external stimuli. Supportively, Braunstein et al. (2016) revealed that breast cancer cells with downregulated H2A and H2B were more sensitive toward anthracycline-induced apoptosis. Collectively, the deregulation of H2AFX may disrupt the DNA replication process, DNA damage repair, and chromosomal stability in both cell lines treated with MS13. These findings suggest that H2AFX may interfere with the transcriptional machinery by sensitizing both glioblastoma and neuroblastoma cells toward MS13 treatment, and thus leading to apoptosis.

Besides, the cytoskeletal protein TUBB was found downregulated in U-87 MG and SH-SY5Y cells. Nonetheless, TUBB was only mapped to “Rho GTPase activates IQGAPs” in SH-SY5Y cells but not in U-87 MG cells. The signaling by Rho GTPases regulates cell shape, cell proliferation, cell adhesion, and cell migration. Given that the cytoskeletal proteins, including microtubules, are essential in regulating cellular processes such as cell division, migration, and intracellular transport, the mutations or alterations in the expression and stability of these proteins were associated with cancer progression (Ong et al., 2020). Therefore, tubulins are promising therapeutic targets in treating cancer. Taxanes and vincristines are two most notable chemotherapeutic drugs that were reported to induce cancer cell death by arresting the cells at mitotic phase by targeting microtubules such as TUBB at the mitotic phase (Kavallaris, 2010). As microtubule assembly underpins the structural integrity of cells and facilitate cell cycle progression (Hall, 2009; Chen and Xie, 2018), downregulation of TUBB by MS13 may inhibit cell migration, disrupt cell integrity, and subsequently lead to cell cycle arrest and apoptosis in glioblastoma and neuroblastoma cells.

Protein SET, formerly known as Oncoprotein 17, was downregulated in MS13-treated U-87 MG and SH-SY5Y. Notably, the overexpression of SET has been associated with poor prognosis, high recurrence rate, and chemoresistance (Cristóbal et al., 2015) in several types of cancer including lung (Liu et al., 2015), glioblastoma (He et al., 2016), breast

(Huang et al., 2018), and pancreas (Bhutia et al., 2013). By inhibiting the protein phosphatase 2A (PP2A) activity, SET interferes with the tumor suppressor function of PP2A. This will have an impact on cellular processes such as apoptosis, protein synthesis, signal transduction, and stress response. Additionally, SET also interacts with Rac1 (Switzer et al., 2011) and nm23-H1 (Fan et al., 2003) to regulate cancer metastasis and inhibits p53 to promote cancer stemness (Wang et al., 2016). Therefore, serving as a promising target, SET antagonists such as sphingosine FTY720 (Oaks et al., 2013) was shown to induce anti-proliferative and anti-migratory activities in cancers. As SET was downregulated in both U-87 MG and SH-SY5Y cells, MS13 may also induce its anti-cancer effects in both glioblastoma and neuroblastoma by serving as a SET inhibitor.

CONCLUSION

The curcumin analog, MS13, demonstrates potent dose-dependent cytotoxicity, and time- and dose-dependent anti-proliferative activity in both U-87 MG and SH-SY5Y cells, over its parent compound, curcumin. MS13 also induces caspase-3 and mitochondrial-dependent apoptosis in both cells. The proteomic analysis of these cells following treatment with MS13 has revealed several common DEPs, i.e., ENO1, HSP90AA1, HSP90AB1, EIF5A, HNRNPK, TUBB, H2AFX, and SET and common top enriched pathways, i.e., “Glycolytic” and “Post-translational protein modification” pathways. Collectively, our current findings suggest that MS13 may induce its cytotoxicity, anti-proliferation, anti-migration, and apoptosis activities in human glioblastoma and neuroblastoma cells via the regulation of DEPs through PPI and specific pathways. These findings derived from proteomics analysis warrants further investigation to uncover the anti-cancer effects of MS13 on these cells in a holistic view.

DATA AVAILABILITY STATEMENT

The datasets presented in this study can be found in online repositories. The names of the repository/repositories and accession number(s) can be found below: The mass spectrometry proteomics data have been deposited to the ProteomeXchange Consortium via the PRIDE [1] partner repository with the dataset identifiers PXD024565 (Glioblastoma) and PXD024564 (Neuroblastoma).

AUTHOR CONTRIBUTIONS

RN was in charge of the conceptualization, methodology, supervision, visualization and writing, reviewing, and editing of the manuscript. PR and IO did the supervision and writing, reviewing, and editing of the manuscript. FA provided the resources. YL was responsible for the investigation, formal analysis, data curation, and preparation, and writing

of the original draft. All authors contributed to the article and approved the submitted version.

FUNDING

This research was funded by Fundamental Research Grant Scheme (FRGS/1/2016/SKK08/MUSM/02/1) under the Ministry of Education (MOE), Malaysia.

ACKNOWLEDGMENTS

The authors would like to acknowledge the Jeffrey Cheah School of Medicine and Health Sciences, Monash University

Malaysia, for the research facilities and support and the LCMS/MS Platform, Monash University Malaysia, for processing the proteomic sample. YL would also like to acknowledge Jeffrey Cheah School of Medicine and Health Sciences, Monash University Malaysia, for providing the scholarship.

SUPPLEMENTARY MATERIAL

The Supplementary Material for this article can be found online at: <https://www.frontiersin.org/articles/10.3389/fmolb.2021.645856/full#supplementary-material>

REFERENCES

- Adams, J. M., and Cory, S. (2018). The BCL-2 arbiters of apoptosis and their growing role as cancer targets. *Cell Death Differ.* 25, 27–36. doi: 10.1038/cdd.2017.161
- Bandino, A., Geerts, D., Koster, J., and Bachmann, A. S. (2014). Deoxyhypusine synthase (DHPS) inhibitor GC7 induces p21/Rb-mediated inhibition of tumor cell growth and DHPS expression correlates with poor prognosis in neuroblastoma patients. *Cell. Oncol.* 37, 387–398. doi: 10.1007/s13402-014-0201-9
- Bhutia, Y. D., Hung, S. W., Krentz, M., Patel, D., Lovin, D., Manoharan, R., et al. (2013). Differential processing of let-7 a precursors influences RRM2 expression and chemosensitivity in pancreatic cancer: role of LIN-28 and SET oncoprotein. *PLoS One* 8:e53436. doi: 10.1371/journal.pone.0053436
- Boland, K., Flanagan, L., and Prehn, J. H. (2013). Paracrine control of tissue regeneration and cell proliferation by Caspase-3. *Cell Death Dis.* 4:e725. doi: 10.1038/cddis.2013.250
- Braunstein, M., Liao, L., Lyttle, N., Lobo, N., Taylor, K. J., Krzyzanowski, P. M., et al. (2016). Downregulation of histone H2A and H2B pathways is associated with anthracycline sensitivity in breast cancer. *Breast Cancer Res.* 18, 1–16.
- Calderwood, S. K., and Murshid, A. (2017). Molecular chaperone accumulation in cancer and decrease in Alzheimer's disease: the potential roles of HSF1. *Front. Neurosci.* 11:192. doi: 10.3389/fnins.2017.00192
- Cen, L., Hutzen, B., Ball, S., DeAngelis, S., Chen, C. L., Fuchs, J. R., et al. (2009). New structural analogues of curcumin exhibit potent growth suppressive activity in human colorectal carcinoma cells. *BMC Cancer* 9:99. doi: 10.1186/1471-2407-9-99
- Chattopadhyay, I., Biswas, K., Bandyopadhyay, U., and Banerjee, R. K. (2004). Turmeric and curcumin: biological actions and medicinal applications. *Curr. Sci.* 87, 44–53.
- Chedotal, A., Kerjan, G., and Moreau-Fauvarque, C. (2005). The brain within the tumor: new roles for axon guidance molecules in cancers. *Cell Death Differ.* 12, 1044–1056. doi: 10.1038/sj.cdd.4401707
- Chen, C., Zhang, B., Wu, S., Song, Y., and Li, J. (2018). Knockdown of EIF5A2 inhibits the malignant potential of non-small cell lung cancer cells. *Oncol. Lett.* 15, 4541–4549.
- Chen, M., and Xie, S. (2018). Therapeutic targeting of cellular stress responses in cancer. *Thorac. Cancer* 9, 1575–1582. doi: 10.1111/1759-7714.12890
- Chikhirzhina, E., Starkova, T., and Polyanchko, A. (2018). The role of linker histones in chromatin structural organization. 1. H1 family histones. *Biophysic* 63, 858–865. doi: 10.1134/s0006350918060064
- Choudhuri, T., Pal, S., Aggarwal, M. L., Das, T., and Sa, G. (2002). Curcumin induces apoptosis in human breast cancer cells through p53-dependent Bax induction. *FEBS Lett.* 512, 334–340. doi: 10.1016/s0014-5793(02)02292-5
- Citalingam, K., Abas, F., Lajis, N. H., Othman, I., and Naidu, R. (2015). Anti-proliferative effect and induction of apoptosis in androgen-independent human prostate cancer cells by 1, 5-bis (2-hydroxyphenyl)-1, 4-pentadiene-3-one. *Molecules* 20, 3406–3430. doi: 10.3390/molecules20023406
- Cristóbal, I., Rincón, R., Manso, R., Caramés, C., Zazo, S., Madoz-Gúrpide, J., et al. (2015). Deregulation of the PP2A inhibitor SET shows promising therapeutic implications and determines poor clinical outcome in patients with metastatic colorectal cancer. *Clin. Cancer Res.* 21, 347–356. doi: 10.1158/1078-0432.ccr-14-0724
- de Weille, J. (2014). On the genesis of neuroblastoma and glioma. *Int. J. Brain Sci.* 2014:217503. doi: 10.1155/2014/217503
- Delgado-López, P., and Corrales-García, E. (2016). Survival in glioblastoma: a review on the impact of treatment modalities. *Clin. Transl. Oncol.* 18, 1062–1071. doi: 10.1007/s12094-016-1497-x
- Faião-Flores, F., Suarez, J. A. Q., Soto-Cerrato, V., Espona-Fiedler, M., Pérez-Tomás, R., and María, D. A. (2013). Bcl-2 family proteins and cytoskeleton changes involved in DM-1 cytotoxic effect on melanoma cells. *Tumor Biol.* 34, 1235–1243. doi: 10.1007/s13277-013-0666-6
- Fan, Z., Beresford, P. J., Oh, D. Y., Zhang, D., and Lieberman, J. (2003). Tumor suppressor NM23-H1 is a granzyme A-activated DNase during CTL-mediated apoptosis, and the nucleosome assembly protein SET is its inhibitor. *Cell* 112, 659–672. doi: 10.1016/s0092-8674(03)00150-8
- Gupta, A., and Dwivedi, T. (2017). A simplified overview of World Health Organization classification update of central nervous system tumors 2016. *J. Neurosci. Rural Pract.* 8, 629–641. doi: 10.4103/jnrp.jnrp_168_17
- Gupta, M. K., Polisetty, R. V., Ramamoorthy, K., Tiwary, S., Kaur, N., Uppin, M. S., et al. (2013). Secretome analysis of glioblastoma cell line-HNGC-2. *Mol. Biosyst.* 9, 1390–1400. doi: 10.1039/c3mb25383j
- Hall, A. (2009). The cytoskeleton and cancer. *Cancer Metastasis Rev.* 28, 5–14.
- He, K., Shi, L., Jiang, T., Li, Q., Chen, Y., and Meng, C. (2016). Association between SET expression and glioblastoma cell apoptosis and proliferation. *Oncol. Lett.* 12, 2435–2444. doi: 10.3892/ol.2016.4951
- Hosoya, T., Nakata, A., Yamasaki, F., Abas, F., Shaari, K., Lajis, N. H., et al. (2012). Curcumin-like diarylpentanoid analogues as melanogenesis inhibitors. *J. Nat. Med.* 66, 166–176. doi: 10.1007/s11418-011-0568-0
- Huang, T. Y., Tsai, T. H., Hsu, C. W., and Hsu, Y. C. (2010). Curcuminoids suppress the growth and induce apoptosis through caspase-3-dependent pathways in glioblastoma multiforme (GBM) 8401 cells. *J. Agric. Food Chem.* 58, 10639–10645. doi: 10.1021/jf1016303
- Huang, Y. H., Chu, P. Y., Chen, J. L., Huang, C. T., Lee, C. H., Lau, K. Y., et al. (2018). SET overexpression is associated with worse recurrence-free survival in patients with primary breast cancer receiving adjuvant tamoxifen treatment. *Clin. Med.* 7:245. doi: 10.3390/jcm7090245
- Jaiswal, A. S., Marlow, B. P., Gupta, N., and Narayan, S. (2002). β -catenin-mediated transactivation and cell-cell adhesion pathways are important in curcumin (diferulylmethane)-induced growth arrest and apoptosis in colon cancer cells. *Oncogene* 21, 8414–8427. doi: 10.1038/sj.onc.1205947
- Kalkavan, H., and Green, D. R. (2018). MOMP, cell suicide as a BCL-2 family business. *Cell Death Differ.* 25, 46–55. doi: 10.1038/cdd.2017.179

- Karmakar, S., Banik, N. L., and Ray, S. K. (2007). Curcumin suppressed anti-apoptotic signals and activated cysteine proteases for apoptosis in human malignant glioblastoma U87MG cells. *Neurochem. Res.* 32, 2103–2113. doi: 10.1007/s11064-007-9376-z
- Kavallaris, M. (2010). Microtubules and resistance to tubulin-binding agents. *Nat. Rev. Cancer* 10, 194–204. doi: 10.1038/nrc2803
- Kim, J., Han, J., Jang, Y., Kim, S. J., Lee, M. J., Ryu, M. J., et al. (2015). High-capacity glycolytic and mitochondrial oxidative metabolisms mediate the growth ability of glioblastoma. *Int. J. Oncol.* 47, 1009–1016. doi: 10.3892/ijo.2015.3101
- Kim, J. H., Paek, K. Y., Choi, K., Kim, T. D., Hahm, B., Kim, K. T., et al. (2003). Heterogeneous nuclear ribonucleoprotein C modulates translation of c-myc mRNA in a cell cycle phase-dependent manner. *Mol. Cell Biol.* 23, 708–720. doi: 10.1128/mcb.23.2.708-720.2003
- Krueger, K. E., and Srivastava, S. (2006). Posttranslational protein modifications: current implications for cancer detection, prevention, and therapeutics. *Mol. Cell. Proteomics* 5, 1799–1810.
- Kuttan, R., Bhanumathy, P., Nirmala, K., and George, M. C. (1985). Potential anticancer activity of turmeric (*Curcuma longa*). *Cancer Lett.* 29, 197–202. doi: 10.1016/0304-3835(85)90159-4
- Li, D., Wang, X., Mei, H., Fang, E., Ye, L., Song, H., et al. (2018). Long noncoding RNA pancEts-1 promotes neuroblastoma progression through hnRNPK-mediated β -catenin stabilization. *Cancer Res.* 78, 1169–1183. doi: 10.1158/0008-5472.can-17-2295
- Li, H., Yang, F., Hu, A., Wang, X., Fang, E., Chen, Y., et al. (2019). Therapeutic targeting of circ-CUX1/EWSR1/MAZ axis inhibits glycolysis and neuroblastoma progression. *EMBO Mol. Med.* 11:e10835. doi: 10.15252/emmm.201910835
- Li, R., Soosairajah, J., Harari, D., Citri, A., Price, J., Ng, H. L., et al. (2006). Hsp90 increases LIM kinase activity by promoting its homo-dimerization. *FASEB J.* 20, 1218–1220. doi: 10.1096/fj.05-5258fje
- Liang, G., Shao, L., Wang, Y., Zhao, C., Chu, Y., Xiao, J., et al. (2009). Exploration and synthesis of curcumin analogues with improved structural stability both in vitro and in vivo as cytotoxic agents. *Bioorg. Med. Chem.* 17, 2623–2631. doi: 10.1016/j.bmc.2008.10.044
- Lin, Y. G., Marlow, B. P., Gupta, N., and Narayan, S. (2007). Curcumin inhibits tumor growth and angiogenesis in ovarian carcinoma by targeting the nuclear factor- κ B pathway. *Clin. Cancer Res.* 13, 3423–3430. doi: 10.1158/1078-0432.ccr-06-3072
- Liu, H., Gu, Y., Wang, H., Yin, J., Zheng, G., Zhang, Z., et al. (2015). Overexpression of PP2A inhibitor SET oncoprotein is associated with tumor progression and poor prognosis in human non-small cell lung cancer. *Oncotarget* 6, 14913–14925. doi: 10.18632/oncotarget.3818
- Liu, H., Liang, Y., Wang, L., Tian, L., Song, R., Han, T., et al. (2012). In vivo and in vitro suppression of hepatocellular carcinoma by EF24, a curcumin analog. *PLoS One* 7:e48075. doi: 10.1371/journal.pone.0048075
- Liu, Y., Tseng, M., Perdreau, S. A., Rossi, F., Antonescu, C., Besmer, P., et al. (2007). Histone H2AX is a mediator of gastrointestinal stromal tumor cell apoptosis following treatment with imatinib mesylate. *Cancer Res.* 67, 2685–2692. doi: 10.1158/0008-5472.can-06-3497
- Louis, D. N., Ohgaki, H., Wiestler, O. D., Cavenee, W. K., Burger, P. C., Jouvett, A., et al. (2007). The 2007 WHO classification of tumours of the central nervous system. *Acta Neuropathol.* 114, 97–109. doi: 10.1007/978-94-007-1399-4_10
- Mathews, M. B., and Hershey, J. W. (2015). The translation factor eIF5A and human cancer. *Biochim. Biophys. Acta Gene Regul. Mech.* 1849, 836–844. doi: 10.1016/j.bbgrm.2015.05.002
- Miyakawa, A., Ichimura, K., Schmidt, E., Varmeh-Ziaie, S., and Collins, V. (2000). Multiple deleted regions on the long arm of chromosome 6 in astrocytic tumours. *Br. J. Cancer* 82, 543–549. doi: 10.1054/bjoc.1999.0961
- Mosmann, T. (1983). Rapid colorimetric assay for cellular growth and survival: application to proliferation and cytotoxicity assays. *J. Immunol. Methods* 65, 55–63. doi: 10.1016/0022-1759(83)90303-4
- Oaks, J. J., Santhanam, R., Walker, C. J., Roof, S., Harb, J. G., Ferencik, G., et al. (2013). Antagonistic activities of the immunomodulator and PP2A-activating drug FTY720 (Fingolimod, Gilenya) in Jak2-driven hematologic malignancies. *Blood* 122, 1923–1923. doi: 10.1182/blood-2013-03-492181
- Ohuri, H., Yamakoshi, H., Tomizawa, M., Shibuya, M., Kakudo, Y., Takahashi, A., et al. (2006). Synthesis and biological analysis of new curcumin analogues bearing an enhanced potential for the medicinal treatment of cancer. *Mol. Cancer Ther.* 5, 2563–2571. doi: 10.1158/1535-7163.mct-06-0174
- Ong, M. S., Deng, S., Halim, C. E., Cai, W., Tan, T. Z., Huang, R. Y. J., et al. (2020). Cytoskeletal proteins in cancer and intracellular stress: a therapeutic perspective. *Cancers* 12:238. doi: 10.3390/cancers12010238
- Paulraj, F., Abas, F., Lajis, N. H., Othman, I., Hassan, S. S., and Naidu, R. (2015). The curcumin analogue 1, 5-bis (2-hydroxyphenyl)-1, 4-pentadiene-3-one induces apoptosis and downregulates E6 and E7 oncogene expression in HPV16 and HPV18-infected cervical cancer cells. *Molecules* 20, 11830–11860. doi: 10.3390/molecules200711830
- Perry, M. C., Demeule, M., Régina, A., Moudjian, R., and Béliveau, R. (2010). Curcumin inhibits tumor growth and angiogenesis in glioblastoma xenografts. *Mol. Nutr. Food Res.* 54, 1192–1201.
- Preukschas, M., Hagel, C., Schulte, A., Weber, K., Lamszus, K., Sievert, H., et al. (2012). Expression of eukaryotic initiation factor 5A and hypusine forming enzymes in glioblastoma patient samples: implications for new targeted therapies. *PLoS One* 7:e43468. doi: 10.1371/journal.pone.0043468
- Qu, W., Xiao, J., Zhang, H., Chen, Q., Wang, Z., Shi, H., et al. (2013). B19, a novel monocarbonyl analogue of curcumin, induces human ovarian cancer cell apoptosis via activation of endoplasmic reticulum stress and the autophagy signaling pathway. *Int. J. Biol. Sci.* 9, 766–777. doi: 10.7150/ijbs.5711
- Switzer, C. H., Cheng, R. Y., Vitek, T. M., Christensen, D. J., Wink, D. A., and Vitek, M. P. (2011). Targeting SET/I 2 PP2A oncoprotein functions as a multi-pathway strategy for cancer therapy. *Oncogene* 30, 2504–2513. doi: 10.1038/ncr.2010.622
- Tomolonis, J. A., Agarwal, S., and Shohet, J. M. (2018). Neuroblastoma pathogenesis: deregulation of embryonic neural crest development. *Cell Tissue Res.* 372, 245–262. doi: 10.1007/s00441-017-2747-0
- Wang, D., Kon, N., Lasso, G., Jiang, L., Leng, W., Zhu, W. G., et al. (2016). Acetylation-regulated interaction between p53 and SET reveals a widespread regulatory mode. *Nature* 538, 118–122. doi: 10.1038/nature19759
- Warburg, O. (1956). On the origin of cancer cells. *Science* 123, 309–314.
- Wu, L., Zhu, X., Song, Z., Guo, M., Liang, J., and Yan, D. (2020). FGD5-AS1 facilitates glioblastoma progression by activation of Wnt/ β -catenin signaling via regulating miR-129-5p/HNRNP axis. *Life Sci.* 256:117998. doi: 10.1016/j.lfs.2020.117998
- Yoshida, T., Maruyama, T., Miura, M., Inoue, M., Fukuda, K., Shimazu, K., et al. (2018). Dietary intake of pyrolyzed deketene curcumin inhibits gastric carcinogenesis. *J. Funct. Foods* 50, 192–200. doi: 10.1016/j.jff.2018.09.033
- Yu, Q., Jianfen, M., Xiaoyi, G., Jun, S., Yongtao, Y., Boqiang, C., et al. (2015). Curcumin enhances the radiosensitivity of U87 cells by inducing DUSP-2 up-regulation. *Cell Physiol. Biochem.* 35, 1381–1393. doi: 10.1159/000373959
- Yusuf, M., Leung, K., Morris, K. J., and Volpi, E. V. (2013). Comprehensive cytogenomic profile of the in vitro neuronal model SH-SY5Y. *Neurogenetics* 14, 63–70. doi: 10.1007/s10048-012-0350-9
- Zanotto-Filho, A., Braganhol, E., Edelweiss, M. I., Behr, G. A., Zanin, R., Schröder, R., et al. (2012). The curry spice curcumin selectively inhibits cancer cells growth in vitro and in preclinical model of glioblastoma. *J. Nutr. Biochem.* 23, 591–601. doi: 10.1016/j.jnutbio.2011.02.015

Conflict of Interest: The authors declare that the research was conducted in the absence of any commercial or financial relationships that could be construed as a potential conflict of interest.

Copyright © 2021 Lee, Rajadurai, Abas, Othman and Naidu. This is an open-access article distributed under the terms of the Creative Commons Attribution License (CC BY). The use, distribution or reproduction in other forums is permitted, provided the original author(s) and the copyright owner(s) are credited and that the original publication in this journal is cited, in accordance with accepted academic practice. No use, distribution or reproduction is permitted which does not comply with these terms.